THE ASTROPHYSICAL JOURNAL, 555:92–105, 2001 July 1

EARLY METAL ENRICHMENT OF THE INTERGALACTIC MEDIUM BY PREGALACTIC OUTFLOWS

PIERO MADAU,[1,2,3] ANDREA FERRARA,[2,4] AND MARTIN J. REES[1]

Received 2000 October 13; accepted 2001 February 21

ABSTRACT

We assess supernova-driven pregalactic outflows as a mechanism for distributing the product of stellar nucleosynthesis over large cosmological volumes prior to the reionization epoch. Supernova (SN) ejecta will escape the grasp of halos with virial temperatures $T_{\rm vir} \gtrsim 10^{4.3}$ K (corresponding to masses $M \gtrsim 10^8$ h^{-1} $M_\odot$ at redshift $z = 9$ when they collapse from 2 σ fluctuations) if rapid cooling can take place, and a significant fraction of their baryonic mass is converted into stars over a dynamical timescale. We study the evolution of SN-driven bubbles as they blow out from subgalactic halos and propagate into the intergalactic medium (IGM), and we show that to lift the halo gas out of the potential well, the energy injection must continue at least until blowaway occurs. If the fraction of ionizing photons that escape the dense sites of star formation into intergalactic space is greater than a few percent, pregalactic outflows will propagate into an IGM that has been prephotoionized by the same massive stars that later explode as SNe, and the expansion of the metal-enriched bubbles will be halted by the combined action of external pressure, gravity, and radiative losses. The collective explosive output of about 10,000 SNe per $M \gtrsim 10^8$ h^{-1} $M_\odot$ halo at these early epochs could pollute vast regions of intergalactic space to a mean metallicity $\langle Z \rangle = \Omega_Z/\Omega_b \gtrsim 0.003$ (comparable to the levels observed in the Lyα forest at $z \approx 3$) without hydrodynamically perturbing the IGM much, i.e., producing large variations of the baryons relative to the dark matter. Rayleigh-Taylor instabilities between the dense shell that contains pristine swept-up material and the hot, metal-enriched, low-density bubble may contribute to the mixing and diffusion of heavy elements. The volume filling factor of the ejecta is higher than 20% if the star formation efficiency is on the order of 10%. Larger filling factors (not required by current observations) may be obtained for larger efficiencies, moderately top-heavy initial mass functions, halos for which a significant fraction of the gas is in a galactic disk and does not couple to the outflow (since matter is ejected perpendicularly to the disk), or from a population of more numerous sources—which would therefore have to originate from lower amplitude peaks. When the filling factor of the ejecta becomes significant, enriched material typically will be at a higher adiabat than expected from photoionization.

Subject headings: cosmology: theory — galaxies: formation — intergalactic medium — quasars: absorption lines

1. INTRODUCTION

In currently popular cosmological scenarios—all of which are variants of the cold dark matter (CDM) cosmogony with different choices for the parameters Ω_M, Ω_Λ, Ω_b, h, σ_8, and n—some time beyond a redshift of 15, the gas within halos with virial temperatures $T_{\rm vir} \gtrsim 10^4$ K [or, equivalently, $M \gtrsim 10^9(1+z)^{-3/2}$ h^{-1} $M_\odot$][5] cooled rapidly, because of the excitation of hydrogen Lyα by the Maxwellian tail of the electron distribution, and fragmented. Massive stars formed with some initial mass function (IMF), synthesized heavy elements, and exploded as Type II supernovae (SNe) after a few times 10^7 yr, enriching the surrounding medium; these subgalactic stellar systems, aided perhaps by an early population of accreting black holes in their nuclei, generated the ultraviolet radiation and mechanical energy that reheated and reionized the universe. While collisional excitation of molecular hydrogen may have allowed the gas in even smaller systems [virial temperatures of only a few hundred kelvin, corresponding to masses around $10^7(1+z)^{-3/2}$ h^{-1} $M_\odot$] to cool and form stars at earlier times (Couchman & Rees 1986; Haiman, Rees, & Loeb 1996; Tegmark et al. 1997), H_2 molecules are efficiently photodissociated by stellar UV radiation, and such "negative feedback" could have suppressed molecular cooling and further star formation inside very small halos (see, e.g., Haiman, Abel, & Rees 2000; Ciardi, Ferrara, & Abel 2000).

Throughout these crucial formative stages, the all-pervading intergalactic medium (IGM) acted as a source for the gas that accretes, cools, and forms stars within these subgalactic systems and as a sink for the metal-enriched material, energy, and radiation that they eject. The well-established existence of heavy elements like carbon, nitrogen, and silicon in the Lyα forest clouds at $z = 3$–3.5 may be the best evidence for such an early episode of pregalactic star formation. The detection of weak but measurable C IV and S IV absorption lines in clouds with H I column densities as low as $10^{14.5}$ cm^{-2} implies a minimum universal metallicity relative to solar in the range [−3.2] to [−2.5] at $z = 3$–3.5 (Songaila 1997). There is no indication in the data of a turnover in the C IV column density distribution down to $N_{\rm C\,IV} \approx 10^{11.7}$ cm^{-2} ($N_{\rm H\,I} \approx 10^{14.2}$ cm^{-2}; Ellison et al. 2000); the analysis of individual pixel optical depths may actually imply the presence of weak metal lines below the detection threshold (Cowie & Songaila 1998; Ellison et al. 2000). Widespread enrichment is further supported by

[1] Institute of Astronomy, Madingley Road, Cambridge, CB3 0HA, UK.
[2] Osservatorio Astrofisico di Arcetri, Largo Enrico Fermi 5, 50125 Firenze, Italy.
[3] Department of Astronomy and Astrophysics, University of California at Santa Cruz, 477 Clark Kerr Hall, Santa Cruz, CA 95064.
[4] Center for Computational Physics, University of Tsukuba, Tsukuba-shi, Ibaraki-ken, 305-8577, Japan.
[5] Throughout this paper we will assume, unless stated otherwise, an Einstein–de Sitter universe with $H_0 = 100\,h$ km s^{-1} Mpc^{-1}.

the recent observations of O VI absorption in low-density regions of the IGM (Schaye et al. 2000).

In this paper we argue that the observed paucity of regions in the IGM that are of truly primordial composition—or have abundances as low as those of the most metal-poor stars in the Milky Way halo (Ryan, Norris, & Beers 1996)—may point to an early enrichment epoch by low-mass subgalactic systems rather than being due to late pollution by massive galaxies. While outflows of metal-rich gas are directly observed in local starbursts (see, e.g., Heckman 1999) and $z \approx 3$ Lyman break galaxies (LGBs; Pettini et al. 2000), most of this gas may not leave these massive galaxies altogether but remains trapped in their gravitational potential wells until it cools and rains back onto the galaxies. By contrast, metal-enriched material from SN ejecta is far more easily accelerated to velocities larger than the escape speed—about 80 km s^{-1} at the center of a $10^8\ h^{-1}\ M_\odot$ Navarro-Frenk-White halo (Navarro, Frenk, & White 1997, hereafter NFW) at $z = 9$—in the shallow potential wells of subgalactic systems (Larson 1974; Dekel & Silk 1986). These early protogalaxies—with masses comparable to those of present-day dwarf elliptical galaxies—are then expected to release significant amounts of kinetic energy, heat, and heavy elements into the surrounding intergalactic gas. Many authors have addressed the impact on the thermal and chemical state of the IGM of SN-driven winds from small starbursting galaxies at high z (e.g., Barkana & Loeb 2001; Ferrara, Pettini, & Shchekinov 2000; Scannapieco & Broadhurst 2001; Mac Low & Ferrara 1999; Murakami & Babul 1999; Nath & Trentham 1997; Voit 1996; Tegmark, Silk, & Evrard 1993) or from massive galaxies at more modest redshifts (Aguirre et al. 2000; Theuns, Mo, & Schaye 2001). Gnedin & Ostriker (1997) and Gnedin (1998) have argued that violent merging between protogalaxies may be an alternative mechanism for transporting metals in the low-density IGM, while Barkana & Loeb (1999) have discussed the possibility that enriched material in halos with virial temperatures $\lesssim 10^4$ K could be photoevaporated at reionization. Here we give an idealized assessment of pregalactic outflows as a mechanism for distributing the products of stellar nucleosynthesis over large volumes. We will be concerned exclusively with explosive multi-SN events operating on the characteristic timescale of a few times 10^7 yr, the lifetime of massive stars. In a complementary study, Efstathiou (2000) has recently shown that a large fraction of the baryonic mass of galaxies with virial temperatures $\approx 10^5$ K can also be expelled in "quiescent" mode, i.e., over the relatively long timescale of 1 Gyr. To anticipate the conclusions of this work, we find that the IGM will be polluted over large scales at the end of the "dark ages" if a fraction greater than a few percent of the baryonic mass of subgalactic halos can be converted into stars over a dynamical timescale. In the case of large star formation efficiencies and/or moderately top-heavy IMFs, the temperatures of vast regions of the IGM will be driven to a higher adiabat than expected from photoionization so as to inhibit in these regions the formation of further protogalaxies by raising the Jeans mass.

2. AN EARLY ENRICHMENT EPOCH?

Before embarking on a discussion of the consequences of pregalactic outflows on the thermal and chemical state of the IGM, it is worth summarizing the following few key observational facts and theoretical results:

1. Numerical N-body/hydrodynamic simulations of structure formation in the IGM within the framework of CDM-dominated cosmologies (e.g., Cen et al. 1994; Zhang, Anninos, & Norman 1995; Hernquist et al. 1996; Theuns et al. 1998) have recently provided a coherent picture of the origin of the Lyα forest: one of an interconnected network of sheets and filaments with virialized systems (halos) located at their points of intersection. The simulations show good agreement with the observed line statistics under the assumption that an IGM with a baryon density parameter $\Omega_b h^2 = 0.019$ (Burles & Tytler 1998) is photoionized and photoheated by a UV background with a hydrogen ionization rate $\Gamma(z = 3.5) \approx 0.6 \times 10^{-12}$ s^{-1}, which is close to that inferred from quasars (Haardt & Madau 1996). They also show a clear correlation between the H I column, gas temperature, and overdensity, with

$$\rho_b/\bar{\rho}_b \simeq 0.8 N_{\rm H\,I,13}^{0.7} \quad \text{and} \quad \rho_b/\bar{\rho}_b \simeq 0.3 T_4^2 \tag{1}$$

at $z = 3.5$ (Ricotti, Gnedin, & Shull 2000; Zhang et al. 1998; Hui & Gnedin 1997).[6] In photoionization equilibrium, an optically thin cloud with internal density ρ_b will have a neutral hydrogen fraction of

$$\frac{n_{\rm H\,I}}{n_{\rm H}} \simeq 10^{-5} \frac{\rho_b}{\bar{\rho}_b} \left(\frac{1+z}{4.5}\right)^3 T_4^{-0.7} \Gamma_{-12.2}^{-1} , \tag{2}$$

where the temperature dependence is from the radiative recombination rate. Combining equations (1) and (2) and omitting for simplicity the redshift and photoionization rate scalings, one obtains approximately $n_{\rm H\,I}/n_{\rm H} \simeq 10^{-5.3} N_{\rm H\,I,13}^{1/2}$. The baryonic mass fraction in the Lyα forest per unit logarithmic H I column interval can be written as

$$f_m = \frac{1.3 m_p}{\Omega_b \rho_{\rm crit}} \frac{N_{\rm H\,I}^2 f(N_{\rm H\,I}, z)}{n_{\rm H\,I}/n_{\rm H}} \frac{dz}{c\,dt} , \tag{3}$$

where m_p is the proton mass, $\rho_{\rm crit} = 3H^2/8\pi G$ is the critical density of the universe at redshift z, $f(N_{\rm H\,I}, z) \simeq 10^{-12.1} N_{\rm H\,I,13}^{-1.5} (1 + z)^{2.5}$ is the bivariate distribution of H I columns and redshifts (cf. Kim et al. 1997), and $c\,dt/dz$ is the line element in a Friedmann cosmology. From these relations, one finds a mass fraction $f_m \simeq 0.6\ h$, which is independent of the H I column; i.e., most of the baryons at this epoch lie in the range $12.5 < \log N_{\rm H\,I} < 14.5$ and are distributed equally per decade in column density (Zhang et al. 1998). The volume filling factor of Lyα forest clouds is

$$f_v = f_m \frac{\bar{\rho}_b}{\rho_b} \approx 0.75 h N_{\rm H\,I,13}^{-0.7} . \tag{4}$$

Hence, in this picture, the metals associated with $\log N_{\rm H\,I} \lesssim 14.2$ filaments fill a fraction $\gtrsim 3\%$ ($h = 0.5$) of intergalactic space and are therefore far away from the high-overdensity peaks where galaxies form, gas cools, and star formation takes place. Their chemical enrichment must then reflect more uniform (i.e., "early") rather than in situ (i.e., "late") metal pollution.

2. At $z = 3$–3.5, clouds with $N_{\rm H\,I} \gtrsim 10^{14.7}$ cm^{-2} show a spread of at most an order of magnitude in their metallicity, and their narrow line widths require that they be photoionized and cold rather than collisionally ionized and hot (Songaila & Cowie 1996). At these redshifts, hot rarefied gas, exposed to a metagalactic ionizing flux, will not be able to cool radiatively within a Hubble time. The cooling time

[6] Throughout this work, we adopt the notation $Y_x = Y/10^x$ and cgs units.

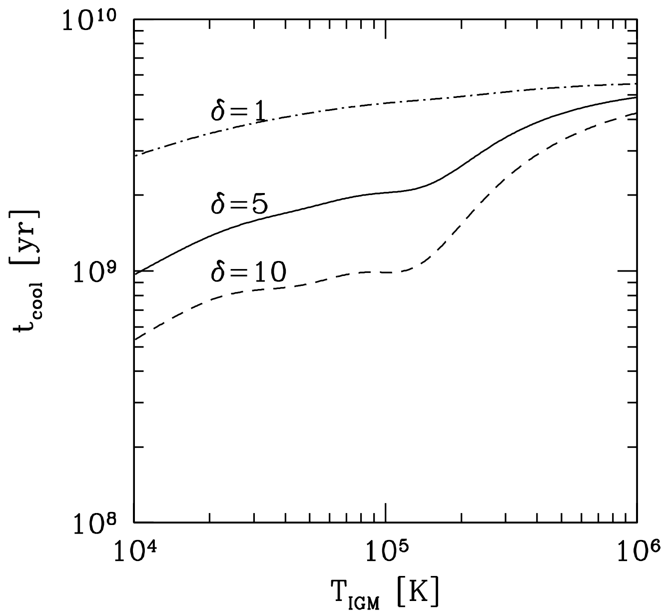

FIG. 1.—Cooling timescale t_{cool} as a function of temperature T_{IGM} for optically thin intergalactic gas at $z = 3.5$. The medium is assumed to have an overdensity of $\delta = \rho_b/\bar{\rho}_b = 1$ (*dash-dotted line*), 5 (*solid line*), and 10 (*dashed line*), primordial abundances, and to be irradiated by a quasar-dominated UV/X-ray background.

can be defined as the ratio of the specific energy content to the radiative cooling rate,

$$t_{cool} = \frac{1.5nkT}{n_H^2 \Lambda} , \quad (5)$$

where k is Boltzmann's constant, T is the gas temperature, and Λ is the radiative cooling function. Here we have computed Λ for a primordial plasma[7] with a helium fraction by mass equal to 0.25 and a total number density of all species n. The cooling function, based on the rates given in Hui & Gnedin (1997), was calculated in the presence of a quasar-dominated UV/X-ray background (Haardt & Madau 1996; Madau & Efstathiou 1999); in this case, the medium is highly photoionized, collisions are not important in determining the ionization structure (although we include them self-consistently), and the collisional excitation cooling of H I and He II becomes ineffective (Efstathiou 1992). The cooling timescale for optically thin intergalactic gas at different overdensities ($\delta \equiv \rho_b/\bar{\rho}_b = 1$, 5, and 10) and redshift $z = 3.5$ is shown in Figure 1: it is longer than or at best comparable to the expansion timescale,

$$\frac{1}{H} = \frac{1}{H_0(1+z)^{3/2}} = 10^9\ h^{-1}\left(\frac{1+z}{4.5}\right)^{-3/2} \text{ yr} , \quad (6)$$

at all temperatures.While it is possible that some metals were dispersed in intergalactic space at late times since hot pressurized bubbles of shocked wind and SN ejecta escaped the grasp of massive galaxy halos and expanded, cooling adiabatically, into the surrounding medium, such a delayed epoch of galactic superwinds would have severely perturbed the IGM (since the kinetic energy of the ejecta is absorbed by intergalactic gas), raising it to a higher adiabat and producing variations of the baryons relative to the dark matter; Lyα forest clouds then would not be expected to closely reflect gravitationally induced density fluctuations in the dark matter distribution, and the success of hydrodynamical simulations in matching the overall observed properties of Lyα absorption systems would have to be largely coincidental.[8] In contrast, the observed narrow Doppler widths could be explained if the ejection of heavy elements at velocities exceeding the small escape speed of subgalactic systems were to take place at very high redshifts. Hot enriched material cools more efficiently at these early epochs since $Ht_{cool} \propto (1+z)^{-3/2}$, and the Compton cooling time of the shocked ionized ejecta off cosmic microwave background (CMB) photons,

$$t_{Comp} = \frac{3m_e c}{4\sigma_T a T_{CMB}^4} = 2.3 \times 10^8\left(\frac{1+z}{10}\right)^{-4} \text{ yr} , \quad (7)$$

is shorter than the expansion timescale. Here m_e is the electron mass, σ_T the Thomson cross section, a the radiation constant, and $T_{CMB} = 2.725(1+z)$ K, which is the temperature of the CMB (Mather et al. 1999). Pregalactic outflows will propagate with typical velocities of a few tens of kilometers per second into a dense IGM that has been prephotoionized by the same massive stars that later explode as SNe, and the expansion of the metal-enriched bubbles will be halted by the external pressure. By $z = 3$, any residual peculiar velocity would have been redshifted away by a factor of 2–3, the Lyα forest would be hydrodynamically "cold," and the intergalactic baryons would have relaxed again under the influence of dark matter gravity.

3. In a CDM universe, structure formation is a hierarchical process in which nonlinear, massive structures grow via the merger of smaller initial units. Large numbers of low-mass galaxy halos are expected to form at early times in these popular cosmogonies, perhaps leading to an era of widespread preenrichment and preheating. The Press & Schechter (1974, hereafter PS) theory for the evolving mass function of dark matter halos predicts a power-law dependence, $dN/d\ln m \propto m^{(n_{eff}-3)/6}$, where n_{eff} is the effective slope of the CDM power spectrum; $n_{eff} \approx -2.5$ on subgalactic scales. As hot, metal-enriched gas from SN-driven winds escapes its host halo, shocks the IGM, and eventually forms a blast wave, it sweeps a region of intergalactic space that increases with the $\frac{3}{5}$ power of the energy E injected into the IGM (in the adiabatic Sedov-Taylor phase). The total fractional volume or porosity, Q, filled by these "metal bubbles" per unit explosive energy density $E\,dN/d\ln m$ is then

$$Q \propto E^{3/5}\, dN/d\ln m \propto (dN/d\ln m)^{2/5} \propto m^{-11/30} . \quad (8)$$

Within this simple scenario, it is the star-forming objects with the smallest masses that will arguably be the most efficient pollutant of the IGM on large scales. Note, however, that since the cooling time of collisionally ionized

[7] At the low metallicities (less than 1% solar) typical of Lyα forest clouds, the thermal behavior can be modeled to a good approximation by a gas with primordial abundances (see, e.g., Sutherland & Dopita 1993).

[8] Assume, for example, that the chemical enrichment of intergalactic gas was due to the numerous populations of LBGs observed at $z = 3$. With a comoving space density above $m_* + 1 = 25.5$ of $0.013\ h^3$ Mpc^{-3} (Steidel et al. 1999), a 1% filling factor would be obtained if each LBG produced a metal-enriched bubble of proper radius equal to about 140 h^{-1} kpc. To fill such a bubble in 5×10^8 yr, the ejecta would have to travel at an average speed close to 600 km s^{-1} (for $h = 0.5$), with characteristic postshock temperatures in excess of 2×10^6 K.

high-density gas in small halos at high redshifts is much shorter than the then Hubble time, virtually all baryons are predicted to sink to the centers of these halos in the absence of any countervailing effect (White & Rees 1978). Efficient feedback is then necessary in hierarchical clustering scenarios to avoid this "cooling catastrophe," i.e., to prevent too many baryons from turning into stars as soon as the first levels of the hierarchy collapse. The required reduction of the stellar birthrate in halos with low circular velocities may result from the heating and expulsion of material due to OB stellar winds and repeated SN explosions from a burst of star formation.

3. BASIC THEORY

3.1. *Dark Matter Halos*

To model the structural properties of subgalactic systems, we will neglect the gravitational potential due to visible mass and assume that virialized dark matter halos, formed through hierarchical clustering, have a universal (spherically averaged) NFW density profile,

$$\rho(r) = \frac{\rho_{\rm crit}\,\delta_c}{cx(1+cx)^2}\,, \tag{9}$$

where $x \equiv r/r_{\rm vir}$, $r_{\rm vir}$ is the "virial" radius of the system, i.e., the radius of the sphere encompassing a mean overdensity of 200, c is the halo concentration parameter, $\delta_c = (200/3)c^3/F(c)$ is a characteristic overdensity, and

$$F(t) \equiv \ln(1+t) - \frac{t}{1+t}\,. \tag{10}$$

The mass of the halo within the virial radius is $M = (4\pi/3)200\rho_{\rm crit}\,r_{\rm vir}^3$. Equation (9) implies a circular velocity

$$v_c^2(r) = \frac{GM(r)}{r} = V_c^2\,\frac{F(cx)}{xF(c)}\,, \tag{11}$$

where $V_c^2 \equiv GM/r_{\rm vir}$. Gas at radius r will escape from the gravitational potential well only if it has a velocity greater than

$$v_e^2(r) = 2\int_r^\infty \frac{GM(r')}{r'^2}\,dr' = 2V_c^2\,\frac{F(cx) + (cx/1+cx)}{xF(c)}\,. \tag{12}$$

The escape speed is maximum at the center of the halo, $v_e^2(0) = 2V_c^2\,c/F(c)$.

To proceed further, we follow the algorithm described in the appendix of NFW and compute the concentration parameter (or, equivalently, the characteristic density contrast δ_c) of dark matter halos as a function of their mass in a standard CDM (SCDM) model with $\Omega_M = 1$, $h = 0.5$, $\sigma_8 = 0.63$, and $n = 1$. The algorithm assigns to each halo of mass M identified at redshift z a collapse redshift $z_{\rm coll}$, defined as the time at which half of the mass of the halo was first contained in progenitors more massive than some fraction of the final mass. The assumption that the characteristic density of a halo is proportional to the critical density at the corresponding $z_{\rm coll}$ implies

$$\delta_c(M,z) \propto \left(\frac{1+z_{\rm coll}}{1+z}\right)^3\,. \tag{13}$$

Since lower mass systems generally collapse at higher redshift, when the mean density of the universe is higher, at any given time, low-mass halos will be more centrally concentrated than high-mass ones. For $M = 10^8\ h^{-1}\ M_\odot$ and $z = 9$, one finds $(z_{\rm coll}, c) = (12.2, 4.8)$. At the same redshift, a $10^9\ M_\odot$ ($10^7\ M_\odot$) halo would have $(z_{\rm coll}, c) = (11.9, 4.7)$ $[(z_{\rm coll}, c) = (12.5, 4.9)]$.

To study in detail the impact on the IGM of an episode of pregalactic star formation at $1 + z \lesssim 10$, we will assume in the following discussion a "typical" concentration parameter of $c = 4.8$. At these epochs, the dark matter halo of a subgalactic system will be characterized by a virial radius

$$r_{\rm vir} = 0.76\ {\rm kpc}\ M_8^{1/3}\ h^{-1}\left(\frac{1+z}{10}\right)^{-1}\,, \tag{14}$$

a circular velocity at $r_{\rm vir}$

$$V_c = 24\ {\rm km\ s^{-1}}\ M_8^{1/3}\left(\frac{1+z}{10}\right)^{1/2}\,, \tag{15}$$

and a virial temperature

$$T_{\rm vir} = \frac{GM}{r_{\rm vir}}\,\frac{\mu m_p}{2k} = 10^{4.5}\ {\rm K}\ M_8^{2/3}\,\mu\left(\frac{1+z}{10}\right)\,, \tag{16}$$

where μ is the mean molecular weight ($\mu = 0.59$ for a fully ionized hydrogen/helium gas) and M_8 is the halo mass in units of $10^8\ h^{-1}\ M_\odot$. The escape speed at the center is

$$v_e(0) = 77\ {\rm km\ s^{-1}}\ M_8^{1/3}\left(\frac{1+z}{10}\right)^{1/2}\,. \tag{17}$$

Note that high-resolution N-body simulations by Bullock et al. (2001) indicate that high-redshift halos are actually less concentrated than expected from the NFW prediction. In this case, we may be slightly overestimating the escape speed from subgalactic systems.

3.2. *Halo Gas Cooling*

If gas collapses and virializes along with the dark matter perturbation to an isothermal distribution, it will be shock-heated to the virial temperature and will settle down to a density profile

$$\ln\rho_{\rm gas}(r) = \ln\rho_0 - \frac{\mu m_p}{2kT_{\rm vir}}\,[v_e^2(0) - v_e^2(r)] \tag{18}$$

(Makino, Sasaki, & Suto 1998). The central gas density ρ_0 is determined by the condition that the total baryonic mass fraction within the virial radius is equal to Ω_b initially,

$$\frac{\rho_0}{\rho_{\rm crit}} = \frac{(200/3)c^3\Omega_b\,e^A}{\int_0^c (1+t)^{A/t}t^2\,dt} = 840\ h^{-2}\,, \tag{19}$$

where $A \equiv 2c/F(c)$. At the virial radius, $\rho_{\rm gas}(r_{\rm vir}) = 0.00144\rho_0$.

Figures 2 and 3 show the cooling function Λ and timescale $t_{\rm cool}$ at the center and the virial radius of an isothermal halo at $z = 9$ as a function of the halo virial temperature. Cooling by Lyα line radiation becomes inefficient for gas temperatures below 2×10^4 K; in a gas of primordial composition at such low temperatures, the main coolant is the radiative de-excitation of the rotational and vibrational states of molecular hydrogen. Objects relying on H_2 cooling are usually referred to as Population III objects. Primordial H_2 is produced with a fractional abundance of $f_{H_2} \approx 2 \times 10^{-6}$ at redshifts $\lesssim 110$ via the H^- formation channel. Starting from this low value, the H_2 abundance increases in

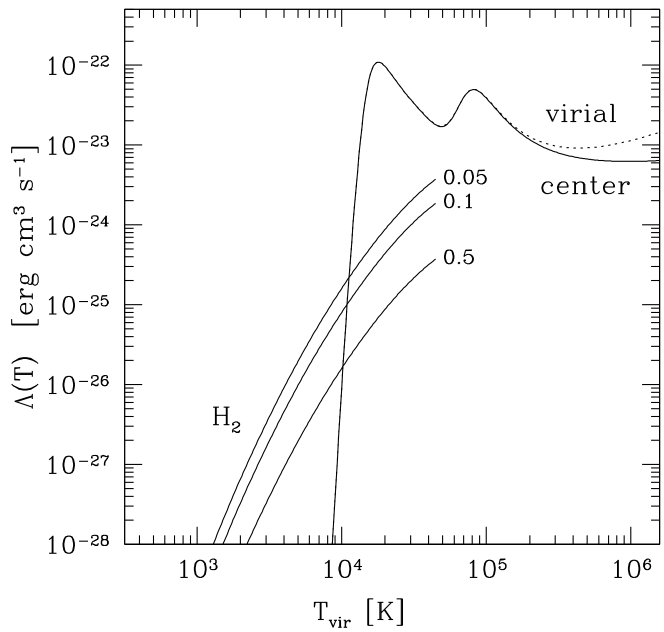

FIG. 2.—Equilibrium cooling rate at the center (*solid lines*) and virial radius (*dashed line*) of an isothermal halo at $z = 9$ as a function of virial temperature T_{vir} and in the absence of a photoionizing background (i.e., prior to the reionization epoch). The halo has an assumed baryonic mass fraction of $\Omega_b = 0.019\ h^{-2}$. The gas density dependence of the cooling function at high temperatures is due to Compton cooling-off comic microwave background photons. The labeled curves extending to low temperatures show the contribution due to H_2 for three assumed values of the metagalactic flux in the Lyman-Werner bands, $4\pi J_{LW}$ (in units of 10^{-21} ergs cm^{-2} s^{-1} Hz^{-1}).

collapsing pregalactic clouds, molecular cooling becomes efficient, and stars can form. While most of the Lyman continuum photons produced by these stars are quickly absorbed by the dense H I disk layers, radiation in the

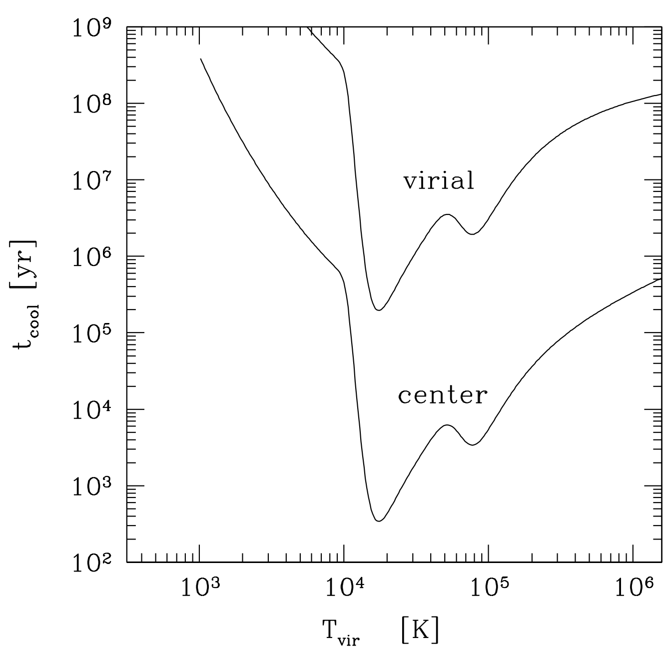

FIG. 3.—Equilibrium cooling time at the center and virial radius of an isothermal halo at $z = 9$ as a function of virial temperature T_{vir} and in the absence of a photoionizing background. Assumptions are as in Fig. 2, with $4\pi J_{LW} = 0.5 \times 10^{-21}$ ergs cm^{-2} s^{-1} Hz^{-1}.

Lyman-Werner bands escapes into the IGM to form a soft-UV cosmic background that can photodissociate H_2 via the Solomon process, thus inhibiting further star formation. An estimate of the H_2 equilibrium fraction under these conditions can be obtained by balancing the rates for the above processes:

$$f_{H_2} = \frac{k_f n_e}{k_d} = 4.8 \times 10^{-9} T_{vir}^{0.88} (4\pi J_{LW,21})^{-1} , \qquad (20)$$

where $J_{LW,21}$ is the specific metagalactic flux in the 11.2–13.6 eV energy range in units of 10^{-21} ergs cm^{-2} s^{-1} Hz^{-1} sr^{-1} and n_e is the residual electron density after recombination, We have taken the formation (k_f) and dissociation (k_d) rates of Abel et al. (1997). Using the above relation, we have included the contribution to the cooling rate per particle due to molecular hydrogen (Martin, Schwarz, & Mundy 1996) in halos of different virial temperatures. The derived cooling function and cooling timescale at $z = 9$ are depicted in Figures 2 and 3 for different values of $J_{LW,21}$. Note that here and below, we are implicitly assuming that the universe is reionized at a redshift $z < 9$; this is because after reionization occurs, there will be a universal background of photons above 13.6 eV that inhibits the formation of dwarf galaxies both by reducing the cooling rate of gas within halos with $T_{vir} \lesssim 5 \times 10^4$ K and also by suppressing the accretion of high-entropy ionized gas into subgalactic fragments (see, e.g., Efstathiou 1992; Thoul & Weinberg 1996; Gnedin 2000).

The fraction of the baryonic content of a halo that can actually cool and reach the center is determined by the balance between the cooling and dynamical timescales of the systems. As shown in Figure 4, for $4.3 < \log T_{vir} < 5.7$, rapid cooling by atomic hydrogen and ionized helium can occur at these epochs on timescales much shorter than the

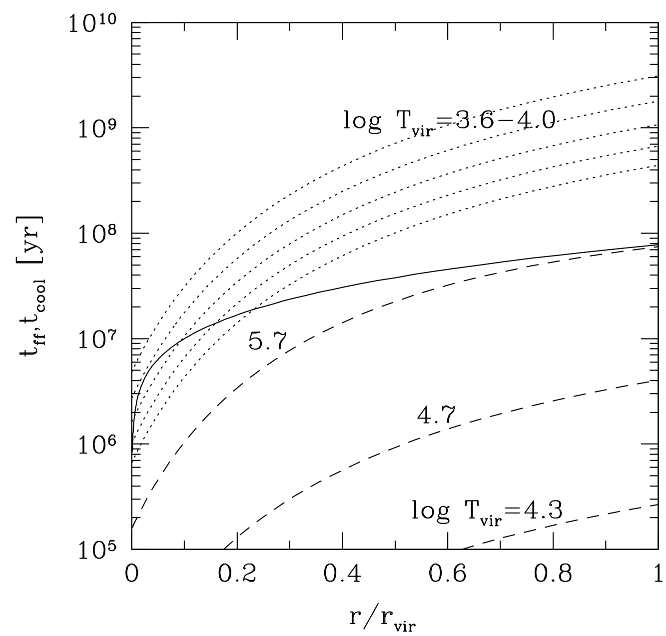

FIG. 4.—Halo cooling times at $z = 9$ as a function of radius for $\log T_{vir} = 4.3, 4.7$, and 5.7 (*dashed curves*). The gas is assumed to be isothermal and in collisional ionization equilibrium. The dotted curves are the same for halos with virial temperatures in the range $3.6 \leq \log T_{vir} \leq 4.0$, in which cooling is dominated by H_2 (the $4\pi J_{LW} = 0.5 \times 10^{-21}$ ergs cm^{-2} s^{-1} Hz^{-1} case). The solid curve is the gravitational free-fall time of an NFW halo at $z = 9$ ($h = 0.5$).

free-fall time,

$$t_{\rm ff}(r) = \int_0^r \frac{dr'}{\sqrt{v_e^2(r') - v_e^2(r)}} = 2.2 \times 10^7\ h^{-1}\ {\rm yr}$$
$$\times \left(\frac{1+z}{10}\right)^{-3/2} \int_0^x dx'[\mathscr{F}(cx') - \mathscr{F}(cx)]^{-1/2}\ , \quad (21)$$

for a gas element at all radii $r < r_{\rm vir}$, where $\mathscr{F}(cx) \equiv [F(cx) + cx/(1+cx)]/[xF(c)]$. Therefore, for masses in the range $10^8\ h^{-1}\ M_\odot \lesssim M \lesssim 10^{10}\ h^{-1}\ M_\odot$, infalling gas never comes to hydrostatic equilibrium but collapses to the center at the free-fall rate. Outside this mass range, i.e., when cooling is dominated by H_2 (at the low end) and free-free emission (at the high end), the halo gas can be pressure-supported and form a quasi-static hot atmosphere. If we denote with $r_{\rm cool}$ the radius where the cooling time is equal to the free-fall time, a parameter f_b can now be defined as the ratio between the gas mass within $r_{\rm cool}$ and the total baryonic mass within the virial radius, $\Omega_b M$. This gas fraction is plotted in Figure 5 as a function of virial temperature. In halos with $f_b = 1$, all the accreted gas can cool immediately, and the supply of cold gas for star formation is limited only by the infall rate. Conversely, in systems with $f_b \ll 1$, the supply of cold gas is regulated by the longer cooling timescale everywhere but for a small amount of gas in the very central region of the halo. When weighted with the steep PS mass function, it is the gas at the peak of the cooling curve—i.e., gas in subgalactic systems with masses comparable to the masses of present-day dwarf elliptical galaxies—that may be more readily available to be transformed into stars on short timescales and may give the origin to explosive multi-SN events.

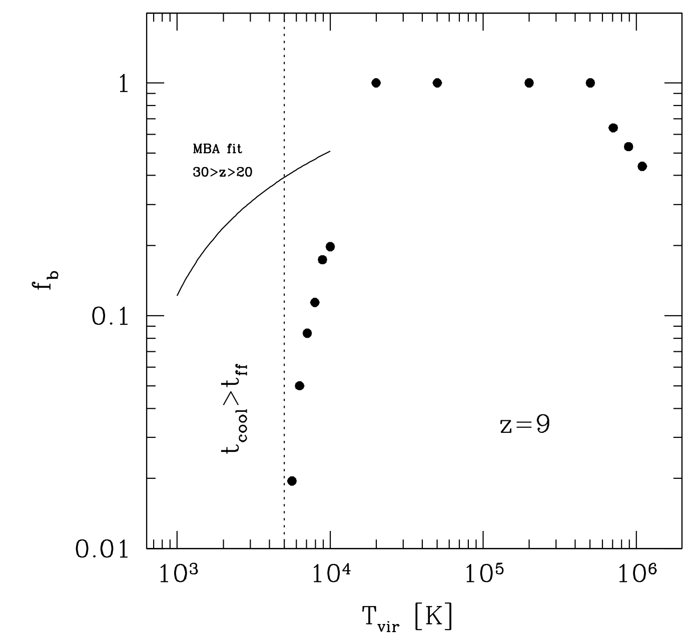

FIG. 5.—Fraction f_b of the total halo gas mass at $z = 9$ that cools faster than the local free-fall time, i.e., that never reaches hydrostatic equilibrium. In halos with $4.3 < \log\ T_{\rm vir} < 5.7, f_b = 1$; i.e., all the accreted gas can cool. For comparison, the fit for f_b derived by Machacek, Bryan, & Abel (2001) from their hydrodynamics simulations is also shown. These numerical results have been obtained in the redshift range $20 \lesssim z \lesssim 30$, in which, because of the higher mean baryon density, the rate of formation of H_2 molecules is much faster than at the redshift of 9 considered here. Some significant differences also arise from the different density and temperature profiles of the Machacek et al. simulated halos. The gas in systems with $T_{\rm vir} < 5000$ K (*dotted vertical line*) cannot cool faster than the local free-fall time at any radius.

In the adopted cosmology (SCDM with $h = 0.5$ and rms mass fluctuation normalized at present to $\sigma_8 = 0.63$ on spheres of 8 h^{-1} Mpc), $M = 10^8\ h^{-1}\ M_\odot$ halos would be collapsing at $z = 9$ from 2 σ fluctuations. At this epoch, more massive halos with $M = 10^{10}\ h^{-1}\ M_\odot$, while able to cool rapidly, would be collapsing from 3 σ peaks and would be too rare to produce significant amounts of heavy elements (in a Gaussian theory, the peaks above 3 σ contain $\sim$5% as much mass as those above 2 σ at a given epoch) unless they were somehow able to form stars more efficiently than lower mass objects. Even if this were the case, however, the SN ejecta would escape the grasp of these more massive halos with less ease, and the fractional volume of the IGM filled by their metal bubbles would be correspondingly small. Halos from 1 σ fluctuations would be more numerous and contain most of the mass, but with virial temperatures of only a few hundred degrees, they would likely be unable to cool ($f_b \ll 1$) via H_2 before reionization actually occurs.

A detailed history of the chemical enrichment of the IGM should include the contribution to its metal content from all levels of the mass hierarchy at every epoch and is beyond the scope of this paper. Recent computations (Haiman et al. 2000; Ciardi et al. 2000; Ricotti et al. 2001) trying to assess the importance of radiative feedback on Population III halos have reached different conclusions. Although it is clear that a soft-UV radiation field tends to prevent the cooling and collapse of these objects and that star formation inside Population III systems shuts off well before reionization, quantifying this effect is difficult since the field intensity depends on poorly known parameters such as the star formation efficiency and the escape fraction of ionizing photons from the star formation sites into the IGM. Additional complications are introduced by locally produced Lyman-Werner photons that photodissociate H_2 molecules in the parent halo gas (Omukai & Nishi 1999) and by hard-radiation components that could boost the formation rate of molecular hydrogen (Haiman et al. 2000) by increasing the electron fraction and thus feeding the H^- formation channel. Given these uncertainties, we will take here a conservative approach and assume that all objects below the critical mass for Lyα efficient cooling are suppressed. Below we will focus on the role played by what we have suggested might be the most efficient pollutant of the IGM on large scales, subgalactic systems with masses $\sim 10^8\ h^{-1}\ M_\odot$ at redshift 9, when large numbers of them become nonlinear and collapse.

3.3. *Energy Injection by SNe*

When gas cools well below its initial virial temperature and infalls to the center, it fragments into clouds and then into stars. Unless the stellar IMF is dramatically bottom-heavy, stars more massive than 8 $M_\odot$ will form in the inner densest (self-gravitating) regions of the halo, eventually releasing their binding energy in an SN explosion, returning most of the metals to the interstellar medium (ISM) and injecting about 10^{51} ergs per event in kinetic energy. We shall assume in the following discussion that (1) all SN explosions take place at the center of the halo and (2) that our stellar population forms in a time interval that is short compared to the lifetime of massive stars. These two simplifying assumptions are delicate and need to be discussed.

The first hypothesis implies spatial coherency among explosions, which in turn ensures that all the energy released by different SNe is used to drive the same "superbubble," producing a cumulative, multi-SN event. This condition is not generally met in large galaxies like our own, where superbubbles occur essentially at random in the disk. For objects with small circular velocities, however, the spatial coherence is essentially guaranteed by the fact that the size of the region where star formation occurs is comparable to or smaller than the characteristic scale of the bubbles. Indeed, if a rotationally supported exponential disk with scale length r_d forms in subgalactic fragments and the specific angular momentum of the disk material is the same as that of the halo, then angular momentum conservation fixes the collapse factor to $r_{\rm vir}/r_d = \sqrt{2}/\lambda$, where λ is the spin parameter of the halo ($\approx$0.05 from N-body simulations; Barnes & Efstathiou 1987), and the equality applies to dark halos treated as singular isothermal spheres. Our fiducial $M = 10^8\ h^{-1}\ M_\odot$ system at $z = 9$ has $r_{\rm vir} = 0.76\ h^{-1}$ kpc and $r_d = 27\ h^{-1}$ pc. If we assume, for simplicity, that the self-gravitating disk of mass M_d follows an isothermal vertical profile with a thermal speed $c_s = 10$ km s^{-1}, which is typical of gas that is continuously photoheated by stars embedded within the disk itself, then its scale height at radius r_d is $h/r_d = (16e)^{1/2}\lambda(M/M_d)(c_s/V_c)^2$, and the disk is rather thick (see, e.g., Wood & Loeb 2000). Within a scale height, the gas density is approximately constant, and the radius R_s of an SN remnant in a uniform medium of density n and in the pressure-driven "snowplow" stage is given by $R_s = (E_{51}/n)^{1/7} t_{\rm yr}^{2/7}$ pc (McKee & Ostriker 1977). It will then take only 10^5 yr for an individual bubble to grow bigger than a disk scale length.

The second assumption has to do with the ability of the collapsing system to transform the cold material into stars on timescales shorter than a few times 10^7 yr, the lifetime of a typical SN progenitor. A larger spread in the stellar birth times is likely to decrease the final number of SNe since ionizing photons from the first massive stars will reheat and ionize the infalling gas, thus inhibiting the formation of subsequent stars. It is difficult to assess the validity of such a hypothesis given our current poor understanding of star formation. While in a typical OB association in the Milky Way, roughly three SN per million years will occur (Heiles 1990), a much higher rate may be sustained in pregalactic systems because of the very short cooling timescale of the halo central regions. If we accept these two assumptions, which can only be met by subgalactic fragments, we can calculate the effects of energy deposition in a star-forming halo. Usually the distinction is made between blowout, a partial removal of the gas from a galaxy, and blowaway, in which the entire gas content is ejected back into the IGM (see, e.g., Mac Low & Ferrara 1999). For a spherical system, as is our admittedly idealized collapsing halo, the two terms are synonymous. Therefore, the superbubble will escape into the IGM only if it can lift out of the halo its entire gas mass. The amount of material transformed into stars can be parameterizedas

$$M_* = \Omega_b\, f_b\, f_* M\ . \tag{22}$$

The cooled fraction of baryons f_b has already been discussed above and found to be equal to unity in such a halo mass range. There are no firm estimates for the star formation efficiency f_*, however, and we consider it a free parameter of our model. We will analyze three limiting scenarios: a low ($f_* = 1\%$), a medium ($f_* = 10\%$), and a high ($f_* = 50\%$) efficiency case. For $h^2\Omega_b = 0.019$ and $h = 0.5$, M_* ranges between 1.5×10^5 and $75 \times 10^5\ M_\odot$. With a comoving space density of dark halos with masses above $10^8\ h^{-1}\ M_\odot$ of about 80 h^3 Mpc^{-3} at $z = 9$ (see § 5), this corresponds to a stellar density parameter of $0.002 f_*$, i.e., between 0.4% and 20% of the total stellar mass inferred at the present epoch (Fukugita, Hogan, & Peebles 1998). We note that, on this assumption, f_* and hence the early luminosity of these systems would exceed that which is predicted by the usual low-mass extrapolation of CDM galaxy formation models (cf. White & Frenk 1991). In these scenarios, f_* is postulated to decline steeply in shallow potential wells, thereby reducing the population of low-luminosity galaxies and avoiding the so-called cooling catastrophe. We also stress that the value $f_* = 50\%$ is only meant to represent an extreme case and really should be considered an upper limit to the star formation efficiency of our fiducial system. This is because when most mechanical energy is injected by SNe after 3×10^7 yr (the main-sequence lifetime of an 8 $M_\odot$ star) and SN-driven bubbles propagate into the galaxy halo, quenching further star formation, only material within $0.4 r_{\rm vir}$ has actually had time to cool, free-fall to the center, and form stars (Fig. 4). With the adopted density profile, the gas within the radius where $t_{\rm ff} = 3 \times 10^7$ yr makes about 40% of the total baryonic mass $\Omega_b M$ of the halo. In general, one would expect significantly lower efficiencies than 50% since the conversion of cold gas into stars is limited by the increasing fractional volume occupied by SN remnants. Additional constraints on f_* may come from the observed metallicity distribution of the most metal-poor stars in the Milky Way halo, although the results will be subject to uncertainties in the low-mass end of the IMF.

The IMF also determines the number of SN events. Conservatively, we assume here a Salpeter IMF, with upper and lower mass cutoffs equal to $M_u = 120\ M_\odot$ and M_l, respectively. The value of M_l is varied from the standard case, $M_l = 0.1\ M_\odot$, to a value appropriate for a top-heavy IMF often predicted for very low metallicity stars, $M_l = 5\ M_\odot$, and up to the extreme case of $M_l = 30\ M_\odot$, in which every star formed explodes as an SN and many of them eventually may end their life as a black hole.

3.4. *Mechanical Luminosity*

The halos under study produce a rather limited amount of very massive stars, and the IMF is then sampled in a stochastic manner. To determine the time-dependent mechanical luminosity injected by SN explosions when a fraction f_* of the gas mass is converted into stars, we have repeatedly sampled the IMF by using a Monte Carlo method until the desired total stellar mass was reached. This procedure yields for $M_l = 0.1\ M_\odot$ and $f_* = (1\%, 10\%, 50\%)$ the following number of stars more massive than 8 $M_\odot$ (hence of SNe): $\mathcal{N} = (1126,\ 11{,}172,\ 55{,}094)$, respectively. For this IMF, one SN occurs every $\nu^{-1} \approx 136$ $M_\odot$ of stars formed, with an average stellar mass $\langle M_s \rangle =$ 0.35 $M_\odot$. For $f_* = 1\%$, the choice $M_l = 5$ (30) $M_\odot$ gives $\mathcal{N} = 6076$ (3000), $\nu^{-1} = 24$ (52) $M_\odot$, and $\langle M_s \rangle = 13.5$ (52.7) $M_\odot$. As we will see later, the differences in the efficiency and IMF will influence the fate and evolution of the ensuing superbubble and its metal content.

To determine the main-sequence lifetime, $t_{\rm OB}(M_s)$, of massive stars, we have used a compilation of the data available in the literature (Schaller et al. 1992; Vacca, Garmany,

& Shull 1996; Schaerer & de Koter 1997; F. Palla 2000, private communication) and derived the approximate fit

$$\frac{t_{\rm OB}(M_s)}{\rm Myr} = \begin{cases} 33\left(\dfrac{M_s}{8\ M_\odot}\right)^{-3/2}, & M_s \leq 28.4\ M_\odot\ , \\ 3.4\left(\dfrac{M_s}{60\ M_\odot}\right)^{-1/2}, & M_s > 28.4\ M_\odot\ . \end{cases} \quad (23)$$

The extrapolation to masses larger than 60 $M_\odot$ is quite uncertain; in general, stars this massive are rare enough that this will not seriously affect our results.

We can now derive the mechanical luminosity of the massive-star association driving the superbubble. Since all stars are assumed to be born coevally in a single burst of star formation, the spread in the SN energy deposition is only due to the difference in $t_{\rm OB}$ for the various masses. The mechanical luminosity is defined as $L(t) = dE/dt$, where E is the energy produced by the ensemble of SNe. We further assume that each SN releases $E_0 = 10^{51}$ ergs in kinetic energy. The derivation naturally accounts for the stochastic behavior of $L(t)$, which nevertheless has two clear features: (1) a pronounced initial peak during the first 5 Myr after the burst that was caused by the crowding of the explosions of the most massive stars, which tend to have very similar ages (see expression for $t_{\rm OB}$ above), and (2) random oscillations around a mean value roughly equal to $\mathcal{N} E_0/\max\ [t_{\rm OB}(M_s)]$.

3.5. *Superbubble Evolution*

In this and the following sections, we will model the evolution of SN-driven bubbles as they blow out from our $10^8\ h^{-1}\ M_\odot$ fiducial halo, allowing for radiative losses, gravity, external pressure, and thermal conduction. Correlated multi-SN explosions will create large holes in the ISM of pregalactic systems, enlarging preexisting ones because of winds from their progenitors stars. Most of the swept-up mass, both in the early adiabatic and in the following radiative phases, is concentrated in a dense shell bounding the hot overpressurized interior, which yet contains enough mass to thermalize the energy input of the SNe.

Superbubbles are canonically studied by using the thin-shell approximation (Kompaneets 1960; Ostriker & McKee 1988), which has been checked against numerical simulations giving excellent agreement (Mac Low & McCray 1988). The shell expansion, whose radius is denoted by R_s, is driven by the internal energy E_b of the hot bubble gas. The pressure of such a gas (with adiabatic index $\gamma = 5/3$) is therefore $P_b = E_b/2\pi R_s^3$. Hence, momentum and energy conservation yield the following relevant equations:

$$\frac{d}{dt}\,(V_s \rho \dot{R}_s) = 4\pi R_s^2 (P_b - P) - \frac{GM(R_s)}{R_s^2}\,\rho V_s\ , \quad (24)$$

$$\frac{dE_b}{dt} = L(t) - 4\pi R_s^2\, P_b\, \dot{R}_s - V_s \bar{n}_{{\rm H},b}^2 \Lambda(\bar{T}_b)\ , \quad (25)$$

where the subscripts "s" and "b" indicate shell and bubble quantities, respectively. We have defined the volume enclosed by the shell as $V_s = (4\pi/3)R_s^3$; the overdots represent time derivatives, and ρ is the pressure of the ambient medium taken to be equal to the halo gas density within $r_{\rm vir}$ and to the IGM background density at $z = 9$ outside the virial radius. As at $r_{\rm vir}$, the halo is still about 60 times denser than the IGM; to avoid unphysical effects due to this jump, we have allowed the two distributions to merge through an exponential transition of width $\Delta = 0.2 r_{\rm vir}$. Finally, $\bar{n}_{{\rm H},b}^2 \Lambda(\bar{T}_b)$ is the cooling rate per unit volume of the hot bubble gas, whose average hydrogen density and temperature are $\bar{n}_{{\rm H},b}$ and $\bar{T}_b$, respectively. The physical interpretation of the various terms is straightforward: in the momentum equation (eq. [24]), the first term on the right-hand side describes the momentum gained by the shell from the SN-shocked wind, while the second term corresponds to the momentum lost to the local gravitational field. The terms on the right-hand side of the energy equation (eq. [25]) describe the mechanical energy input, the work done against the shell, and the energy losses due to radiation.

It is important to remark here that we are actually neglecting the complicated weblike structure ubiquitous to three-dimensional cosmological hydrodynamical simulations (see, e.g., Cen et al. 1994; Zhang et al. 1995). In CDM universes, virialized systems form at the intersection of mildly overdense filaments, along which most of the mass accretion (inflow) actually occurs; outside the virial radius, there will still be a power-law decrease in density within material that is flowing in, but of course the spherical assumption breaks down. Moreover, prior to the reionization epoch, a significant fraction of all baryons is not distributed in a low-density IGM but actually condenses into numerous small halos with virial temperatures above the cosmological Jeans mass. Such "minihalos" have not yet been resolved in large-scale cosmological simulations and are expected to dominate the average gas clumping in the IGM (Haiman, Abel, & Madau 2001). We have also ignored any effects due to possible inhomogeneities within the halo gas. The shallow slope of the CDM spectrum on mass scales $\lesssim 10^8\ M_\odot$ leads to all small-scale fluctuations going nonlinear almost simultaneously in time. The evolution of these early halos will then be marked by frequent mergers, which could raise the gas to a higher adiabat by shock heating and yield complex velocity and density fields within the "virial radius" (Abel, Bryan, & Norman 2000). In this first assessment of pregalactic outflows, we shall assume for simplicity that much of their structure and hydrodynamics can be understood from spherical profiles of the physical quantities.

To determine the pressure P of the ambient medium, we further assume that both the halo gas and the IGM are photoheated at a temperature of 10^4 K by the SN progenitors. In general, the size of an intergalactic H II region around a galaxy halo will depend on the H-ionizing photon luminosity $\dot{N}_i$, the fraction $f_{\rm esc}$ of these photons that can actually escape the dense star formation regions into the IGM, the IGM mean density $\bar{n}_{\rm H}$, and the volume-averaged recombination timescale $\bar{t}_{\rm rec}$. When the source lifetime t_s is much less than $(\bar{t}_{\rm rec}, H^{-1})$, however, as expected for a subgalactic halo shining for a few times 10^7 yr before being blown away by SN explosions (or in the case of a short-lived quasar; Madau & Rees 2000), recombinations can be neglected, and the evolution of the H II region can be decoupled from the Hubble expansion. The radius of the ionized zone is then

$$R_I = \left(\frac{3\dot{N}_i\, f_{\rm esc}\, t_s}{4\pi \bar{n}_{\rm H}}\right)^{1/3} \approx (54\ {\rm kpc}) \left(\frac{\Omega_b h^2}{0.02}\right)^{-1/3} \times \left(\frac{1+z}{10}\right)^{-1} \left(\frac{t_s}{10^7\ {\rm yr}}\right)^{1/3} (\dot{N}_{52}\ f_{\rm esc})^{1/3}\ , \quad 26$$

where $\dot{N}_i = 10^{52} \dot{N}_{52}\ {\rm s}^{-1}$ is the ionizing photon luminosity due to 10^3 massive stars distributed according to a Salpeter

IMF. R_I will then be larger than the final size of the SN-driven superbubble (derived below) for values of the escape fraction greater than a few percent.

It is interesting to derive the timescale at which the postshock gas enters the radiative phase. One can show (Weaver et al. 1977) that when the ambient gas pressure, gravity, and cooling can be neglected and $L(t)$ = constant, the solution of the above equations is

$$R_s = \left(\frac{125}{154\pi}\right)^{1/5}\left(\frac{Lt^3}{\rho}\right)^{1/5} . \tag{27}$$

The temperature of the postshock gas is then

$$T_{\rm ps} = \left(\frac{3\mu m_p}{16k}\right)\dot{R}_s^2 = 4 \times 10^4\left(\frac{L_{38}}{t_{\rm Myr}^2\, n}\right)^{2/5} \text{K} . \tag{28}$$

For $f_* = 1\%$ and $M_l = 0.1\ M_\odot$, one has $L_{38} \equiv L/(10^{38}$ ergs s$^{-1}) \approx 10$; also, in the central region of our fiducial halo, the total gas number density is $n \approx 10$ cm^{-3}. At such temperatures and densities, the cooling rate per particle is $\approx 2 \times 10^{-22}$ ergs s^{-1}. Hence, the cooling time is $t_{\rm cool}(t = 1$ Myr$) \approx 1300$ yr, much shorter than the dynamical time of the system, ensuring that the shell forms very rapidly and justifying the use of the thin-shell approximation. These estimates also highlight the difference between a bubble produced by repeated SNe explosions and a single point explosion. In the former case, most of the energy of the bubble resides in the hot, very inefficiently radiating cavity gas generated by the continuous energy injection, while most of the mass is contained in a thin layer that collapses to form the dense, cool shell.

The final step consists in the determination of the cooling rate of the bubble, which depends on the density and temperature of the hot interior. The thin-shell equations only provide a relation for the product of these two quantities (i.e., the pressure), so another physical relation must be derived. Most of the bubble gas mass comes from the conductive evaporation at the contact surface between the hot gas and the cold shell. The structure of conductive/cooling fronts has been studied by several authors (e.g., Cowie & McKee 1977; McKee & Begelman 1990; Ferrara & Shchekinov 1993). Under the conditions in which thermal conduction is unsaturated, the evaporative flow is steady, radiative losses are negligible, and the rate at which gas is injected from the shell into the cavity is

$$\frac{dM_{\rm ev}}{dt} = \frac{16\pi\mu\eta}{25k}\, T_b^{5/2} R_s = C_1\, T_b^{5/2} R_s , \tag{29}$$

where $\eta = 6 \times 10^{-7}$ (we have assumed a Coulomb logarithm equal to 30) is the classical Spitzer thermal conduction coefficient.

The interior distribution of temperature and density are known to obey a self-similar solution of the type $f(x) = f_c(1 - \zeta)^q$, where $q = \frac{2}{5}\ (-\frac{2}{5})$ if f represents the temperature (density), f_c is the value of the variable at the center, and $\zeta \equiv r/R_s$ (where r is the radial coordinate inside the bubble). According to this solution, $P_b \propto n_b T_b$ = constant, consistent with the hypothesis implicitly made that SN shocks rapidly decay into sound waves inside R_s. By integrating the density profile up to R_s, we obtain the total mass in the bubble, $M_b = C_2 n_b R_s^3$, where $C_2 = (125/39)\pi\mu m_p$. Differentiating this expression with respect to time and equating it to the evaporation rate (eq. [29]), we finally obtain an equation for the evolution of the temperature T_b,

$$\frac{dT_b}{dt} = 3\,\frac{T_b}{R_s}\,\dot{R}_s + \frac{T_b}{P_s}\,\dot{P}_s - \frac{23}{10}\,\frac{C_1}{C_2}\,\frac{kT_b^{9/2}}{R_s^2 P_s} . \tag{30}$$

This relation closes the system equations (24) and (25) and allows us to derive the temperature and density structure of the bubble and its cooling rate.

4. NUMERICAL RESULTS

The evolutionary equations (eqs. [24], [25], and [30]) have been integrated numerically. We start by analyzing the low-efficiency case, $f_* = 1\%$, in some detail to highlight the relevant physics. As shown in Figure 6, the radius of the SN-driven bubble increases with time up to a final stalling value of $R_f = 3.5$ kpc, when pressure equilibrium is achieved. This happens in approximately 180 Myr, less than half of the then Hubble time; up to this point, the evolution is largely unaffected by the Hubble expansion. In the initial stages, we find $R_s \propto t^{1.1}$, a faster growth than given in equation (27), both because of the acceleration occurring in the halo density stratification and, less significantly because of the time-dependent mechanical luminosity. In the late stages of the evolution, the shell evolves according to the snowplow (momentum-conserving) solution, $R_s \propto t^{1/4}$, as expected in the uniform IGM density field. Gas will be lost from the halo if its specific enthalpy exceeds its gravitational binding energy per unit mass. The distinctive feature of blowaway can be seen in the velocity profile as a sudden jump of 10–15 km s^{-1} occurring at $t = 40$ Myr. In all cases, the velocity just before reacceleration is slightly lower than the escape velocity at the virial radius, $v_e(r_{\rm vir}) = 48$ km s^{-1}. The outer shock is radiative as long as it runs into the ISM of the protogalaxy. After breakout ($t = 40$ Myr), the inverse Compton cooling time is 230 Myr, and the shock becomes adiabatic. (Compton cooling dominates since we assume the IGM to be photoionized, and collisional excitation cooling of H and He is accordingly suppressed.) For illustrative purposes, we also show solutions in which the gravity term was turned off, the pressure of the IGM was set to zero, and the halo gas mass was set to 50% of the standard value to mimic the possible presence of a cold galactic disk, which the (bipolar) outflow hardly couples to in numerical simulations (Mac Low & Ferrara 1999). It is only in the last case that the final stalling radius differs significantly from our fiducial solution. Note that, except in the case of zero external pressure, we actually stop the numerical integration of the equation at Mach number $\mathscr{M} = 1$ since the shock decays into sound waves. We define the radius where that happens as the "stalling radius," even if at that point the bubble pressure is still slightly higher than the external pressure of the IGM and the expansion will continue for a while longer. In practice, since the thin-shell approximation assumes a strong shock, our solution actually breaks down before $\mathscr{M} = 1$.

One feature of our model for the evolution of a wind-driven bubble is that conductivity erodes the inside of the cold shell and thereby mixes some swept-up material into the hot cavity. If the SN ejecta carry magnetic fields, then conductivity will be markedly reduced perpendicular to $\boldsymbol{B}$, and this process will be inhibited. To check whether our solution depends crucially on the value of the thermal conduction coefficient, we have run a case in which η in equation (30) was decreased by a factor of 100. We find that the

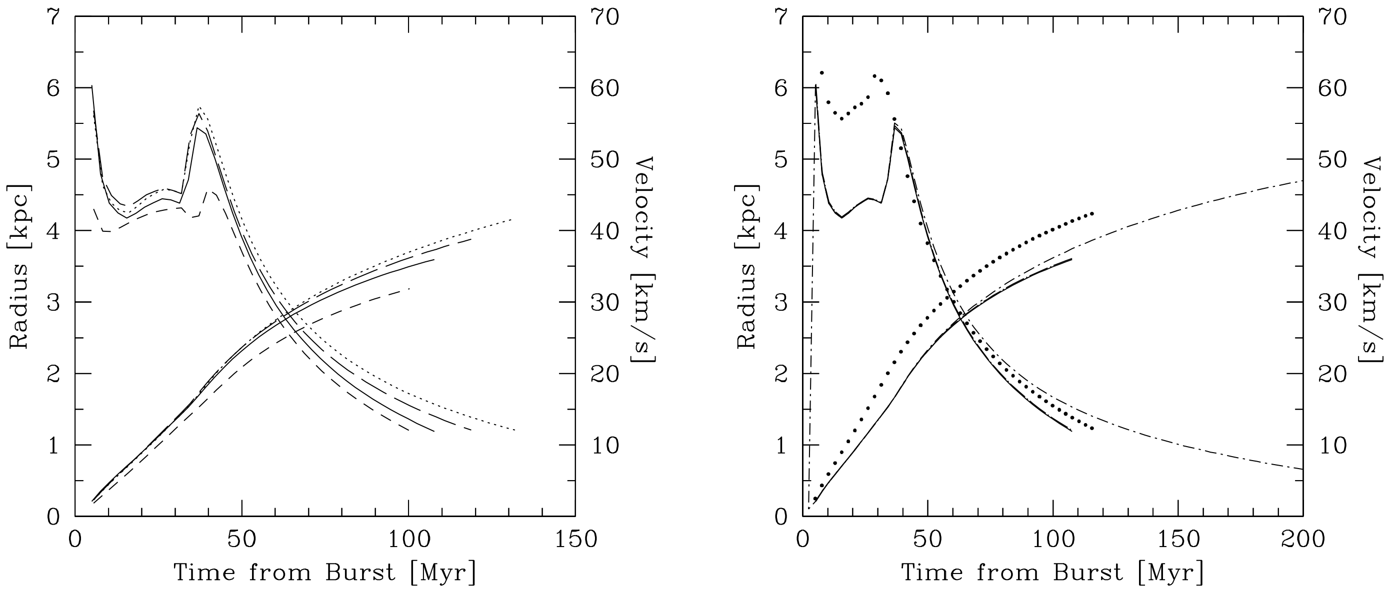

FIG. 6.—Evolution of the shell radius and velocity in the fiducial case $f_* = 1\%$ and $M_l = 0.1\ M_\odot$ (the solid curves *in both panels*, repeated for clarity). All other curves show solutions with the same parameters when in turn: cooling is inhibited (*dotted curves*), the mechanical luminosity is kept at the constant value $L_{38} = 10$ (*short-dashed curves*), gravity is neglected (*long-dashed curves*), the IGM external pressure is set equal to zero (*dot-dashed curves*), and the halo gas mass is 50% of the standard value (*large-dotted curves*). A case with thermal conductivity suppressed by 2 orders of magnitude cannot be distinguished from the solid curve.

temperature profile of the gas within the cavity is increased by less than 25%. Such a change leaves the rate of expansion of the cold shell essentially unaffected by the lower conductivity. This is because the (thermo)dynamics of the bubble is largely determined by the mechanical energy input and adiabatic expansion.

4.1. *Varying the Star Formation Efficiency*

We now explore the effect of varying the star formation efficiency f_*. The results of the numerical calculations are shown in Figure 7. The evolution is qualitatively similar in the three cases, but the final radius is significantly larger as f_* increases; for example, the case $f_* = 10\%$ produces a bubble radius that is 3.3 times larger than for $f_* = 1\%$. Note that now the stalling point is reached only at ages comparable to the then Hubble time t_H, where our Newtonian solution breaks down. In the extreme case of $f_* = 50\%$, the shell is still expanding at a velocity of 30 km s^{-1} at $t = 0.5 t_H = 200$ Myr.

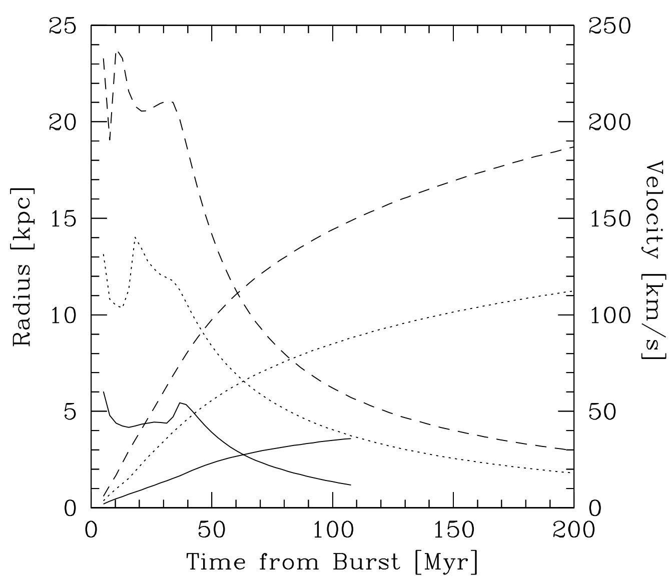

FIG. 7.—Same as Fig. 6, but for the cases $(f_*, M_l) = (1\%, 0.1\ M_\odot)$ (*solid curves*; repeated for comparison), $(10\%, 0.1\ M_\odot)$ (*dotted curves*), and $(50\%, 0.1\ M_\odot)$ (*dashed curves*).

4.2. *Varying the IMF*

Variations in the lower mass cutoff of the adopted Salpeter IMF will also affect our solution. Recall that the number of SNe produced by our three different choices of $M_l = (0.1, 5, 30)\ M_\odot$ is $\mathcal{N} = (1126, 6076, 3000)$, respectively, for $f_* = 1\%$; obviously, in the last case, the progenitor stars are much more massive. The energy released into the ISM by these very high mass SNe may well be lower than assumed here since part of the ejecta may fall back to form a black hole. Even if this is not the case, the ability of very massive SNe to drive outflows is limited because of their short lifetime, as shown in Figure 8. The moderately top-heavy IMF case, $M_l = 5\ M_\odot$, generates a final radius of about 10 kpc, i.e., 2.5 times larger than for $M_l = 0.1\ M_\odot$. For the very top-heavy IMF with $M_l = 30\ M_\odot$, the shell barely reaches 2 kpc in spite of being driven by 2.7 times more SNe than in the fiducial scenario. The reason is that in this case, the pulsed mass and the energy input only last for ≈ 3 Myr, and the increased peak mechanical luminosity ($L_{38} = 10^3$) is not enough to counterbalance the strong external pressure of the dense halo gas: the bubble enters the snowplow phase well before blowing out into the IGM and decelerates rapidly. To lift the halo gas out of the potential well, it is then important that the energy injection continues at least until blowaway occurs; after that, the shell will propagate to large distances while conserving momentum in the rarefied IGM.

4.3. *Bubble Temperature*

The evolution of the gas temperature T_c at the center of the hot, metal-enriched expanding bubble [recall that

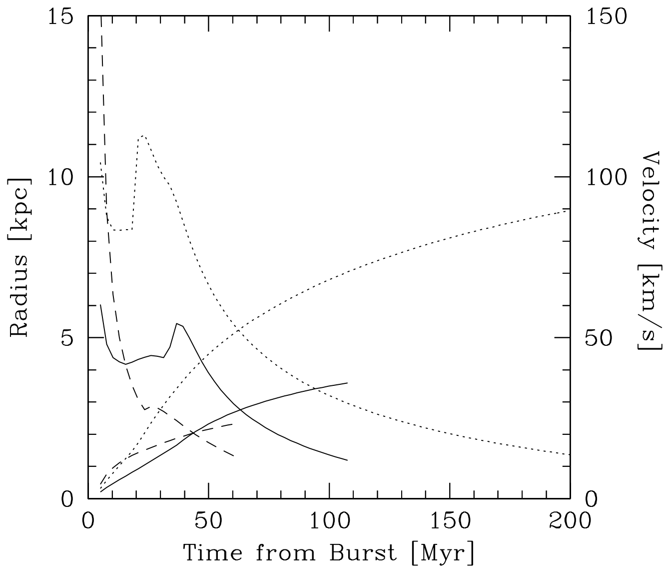

FIG. 8.—Same as Fig. 6, but for the cases $(f_*, M_l) = (1\%, 0.1\ M_\odot)$ (*solid curves*; repeated for comparison), $(1\%, 5\ M_\odot)$ (*dotted curves*), and $(1\%, 30\ M_\odot)$ (*dashed curves*).

$T(r) = T_c(1 - r/R_s)^{2/5}$ inside the cavity] is shown in Figure 9. While a fraction on the order of 10% of the then Hubble time is spent at high temperatures ($\log T_c = 6.6$–7.2), after blowaway cooling sets in very rapidly. This behavior is common to all cases except the most extreme one with $M_l = 30\ M_\odot$, which essentially lacks the first very hot phase. Bubbles that do not stall continue to expand and cool. Inverse Compton cooling is the dominant source of energy loss, as can be inferred from the slope of the temperature profile, which is much steeper than expected from pure adiabatic expansion (in this phase, $R_s \propto t^{1/4}$; hence, $T_c \propto t^{-1/2}$ if the gas is adiabatic). Thus, independently of whether a stalling radius is reached or not, all bubbles will continue to cool according to essentially the same law.

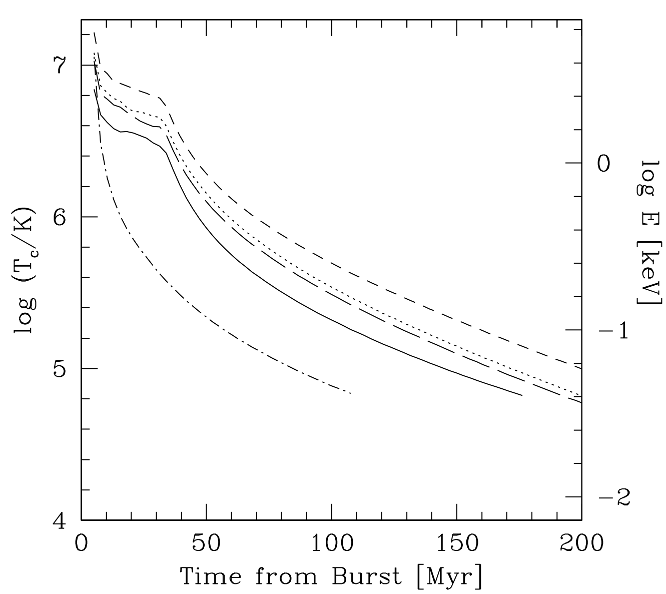

FIG. 9.—Evolution of the gas temperature at the center of the expanding bubble for the five cases $(f_*, M_l) = (1\%, 0.1\ M_\odot)$ (*solid curve*), $(1\%, 5\ M_\odot)$ (*long-dashed curve*), $(1\%, 30\ M_\odot)$ (*dot-dashed curve*), $(10\%, 0.1\ M_\odot)$ (*dotted curve*), and $(50\%, 0.1\ M_\odot)$ (*short-dashed curve*).

5. DISCUSSION

In the previous section, we have modeled the evolution of SN-driven bubbles as they blow out from subgalactic halos and propagate into the IGM prior to the reionization epoch. We have seen that SN ejecta will escape the grasp of halos with virial temperatures $T_{\rm vir} \gtrsim 10^{4.3}$ K at $z = 9$ (when they collapse from 2 σ fluctuations) if a significant fraction of their baryonic mass can be converted into stars over a dynamical timescale. Depending on the star formation efficiency, IMF, and detailed physics of the expansion, we find that after about half of the then Hubble time, these outflows will have produced a warm, 10^5 K, metal-enriched, low-density region, with a size between a few and several 10 times larger than the virial radius of the source halo surrounded by a colder, dense shell that contains most of the swept-up mass. At $t = 10^8$ yr, typical shell bulk velocities range between 12 (for $f_* = 1\%$) and 40 km s^{-1} ($f_* = 10\%$) and up to 60 km s^{-1} ($f_* = 50\%$). If the fraction of ionizing photons that escape the dense sites of star formation into the intergalactic space is greater than a few percent, SN-driven bubbles will propagate into a prephotoionized medium, and their expansion will be halted by external pressure, gravity, and radiative losses. When the velocity of the outflow becomes subsonic, the enriched material gets dispersed by the random velocities in the IGM, and the bubble looses its identity.

Knowing the mass within the bubble and the metal yield per SN, we can now derive the metallicity volution of the bubble. We have used the compilation of Todini & Ferrara (2000)—essentially based on case A of Woosley & Weaver (1995)—who give the chemical composition of the ejecta for zero-metallicity Type II SNe (at redshift 9, the universe may be too young to host Type Ia SNe) as a function of their mass. At each time step of the simulation, we check for the massive stars that became SNe; we sum over the mass of the heavy elements produced by them and divide by the mass of the hot gas within the bubble at that time. This is the typical metallicity inside the bubble if metals can be efficiently mixed within the cavity. Generally speaking, the metal-rich ejecta will be separated from the shell-evaporated gas by a contact discontinuity. The main problem then is to disrupt this surface. When the cooling time in the cavity becomes shorter than its age, a cooled shell will form that rapidly becomes unstable (Gull 1973) to Rayleigh-Taylor (RT) and Kelvin-Helmoltz (KH) instabilities. The "fingers" produced by RT instabilities will penetrate deep into the high-metallicity gas and may be eroded by KH instabilities due to the passage of rapidly moving hot gas, i.e., a mixing layer, perhaps creating a rather uniform distribution of metals inside the bubble.

Further mixing, this time between the shell and the bubble gas, may occur after the expansion stalls. At that time, because of the restoring gravitational force g on the shell from the dark matter halo, the acceleration vector points from the dense shell to the rarefied bubble, an RT unstable situation. The growth time of the RT instability on spatial scales λ_s is

$$t_{\rm RT} \simeq \left[\frac{2\pi g}{\lambda_s}\frac{(\Delta - 1)}{(\Delta + 1)}\right]^{-1/2} \simeq \left(\frac{2\pi g}{\lambda_s}\right)^{-1/2} . \quad (31)$$

If the density contrast between the shell and the hot cavity gas is $\Delta \equiv n_s/n_h \gg 1$ and $g = 3 \times 10^{-11}$ cm s^{-2} at $r = 10$ kpc, then $t_{\rm RT}$ is less than 10 Myr for any reasonable thickness (tens of parsecs) of the shell. Hence, the mixing of shell material with the interior metal-enriched gas may be quite rapid. Ferrara et al. (2000) have recently pointed out that additional processes related to the mixing of the gas caused by time-varying gravitational tidal forces produced by halo interactions must be invoked if the presence of metals at lower redshifts is found to be ubiquitous. The timescale of the process is difficult to estimate since it depends on the peculiar velocities of the halos, which are predicted to be low at high redshift. Note that the metal enrichment of the hot gas inside the bubble will increase its cooling rate, which may become comparable to inverse Compton cooling. This is achieved around metallicity $\approx 0.5\ Z_\odot$ at $z = 9$. While our treatment may then underestimate the cooling rate, we have seen in the previous section that cooling has a weak effect on the overall dynamics of the ejecta.

The time evolution of the bubble average metallicity Z_b is shown in Figure 10 for the five cases studied. Its value is affected by the dynamical evolution of the bubble through the injection by evaporation by mass from the shell into the cavity. At later times, after blowaway, Z_b rapidly approaches a constant value determined by the fact that (1) metal production ceases with the last explosion after $t = 35$ Myr and (2) the evaporative mass flow rate (i.e., the mass input in the bubble) drops, being extremely sensitive ($\propto T^{5/2}$) to the (rapidly decreasing) temperature. The metallicity then becomes the ratio of two constants and is determined by the past dynamical evolution of the outflow. The final values are in the narrow range of $Z_b = 0.2$–$0.4\ Z_\odot$, with the only exception being the peculiar case with $M_l = 30\ M_\odot$, which has $Z_b = 3 \times 10^{-2}\ Z_\odot$. In Table 1 we show the expected bubble and shell masses at stalling. The final ratio M_b/M_s is on the order of 1%. Thus, if the heavy elements were completely mixed into the swept-up shell, then the resultant metallicities would be lower than those derived above by about 2 orders of magnitude. It is possible,

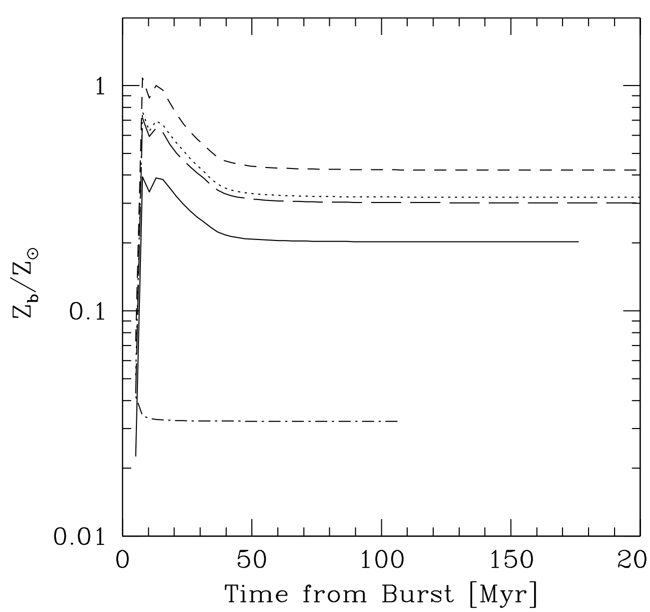

FIG. 10.—Average metallicity of the bubble Z_b (in solar units) for the five cases shown in Fig. 9 as a function of time from the burst. If heavy elements get mixed up with shell material, the mean metallicity of the shell-bubble outflow will be 2 orders of magnitude lower than Z_b.

TABLE 1

BUBBLE AND SHELL MASSES AT STALLING RADIUS

M_l ($M_\odot$)	f_* (%)	M_b ($M_\odot$)	M_s ($M_\odot$)	M_b (M_s) (%)
0.1	1	1.0×10^5	1.6×10^7	0.7
	10	6.8×10^5	5.5×10^7	1.2
	50	2.5×10^6	1.6×10^8	1.5[a]
5........	1	4.0×10^5	3.2×10^7	1.3
30	1	1.0×10^5	1.5×10^7	0.7

[a] Evaluated at $t = 200$ Myr.

though, that the heavy elements may remain restricted to a region with a modest volume filling factor and perhaps would not penetrate into the underdense medium between the halos. As already mentioned, the outcome depends on the onset of RT instabilities; nonlinear development of these instabilities would lead to a more widespread dispersal of the heavy elements through the IGM. The details are sensitive to the sound speed within the bubble when it stalls; this speed depends on how much small-scale internal mixing there has been within the bubble due to conductivity, etc., but it could be substantially higher than the escape velocity. If so, then pressure-driven fingers of hot enriched material (originating within the bubble) could propagate out into the IGM, readily reaching distances on the order of the interhalo spacing if they maintained their identity and did not mix too rapidly. The effectiveness of mixing would depend on the extent to which conductivity is inhibited by magnetic fields. It is worth noting that the bubble material (consisting substantially of SN remnants) may well contain a magnetic field. If so, the dispersal of the first heavy elements and the first ("seed") magnetic fields are intimately connected. If the fingers are magnetized, then they may well propagate a long way before mixing with their surroundings. Whether the intergalactic heavy elements are fully mixed is, however, an interesting question that is still open. The Lyα forest observations imply that most lines of sight through each "cloud" or filament encounter some heavy elements, but it is not clear that the mixing is uniform. It is possible that, even at redshifts of 3–5, the IGM is inhomogeneous on very small scales. Even in the regions that have been enriched, the metals could be restricted to magnetized "streaks" with a volume filling factor of as little as 1%. These would corresponding to the fingers, which we envisage having formed at $z = 10$ (which would have been sheared and distorted by the subsequent gravitational clustering that led to the fully developed forest at $z = 3$–5).

What is the spatial extent of the ensemble of wind-driven ejecta? In the adopted flat cosmology ($\Omega_M = 1$, $h = 0.5$, $\sigma_8 = 0.63$, $n = 1$, and $\Omega_b h^2 = 0.019$) and according to the PS formalism, the comoving abundance of collapsed dark halos with masses $M \approx 10^8\ h^{-1}\ M_\odot$ at $z = 9$ is about 80 h^3 Mpc^{-3}, corresponding to a mean proper distance between neighboring halos of 15 h^{-1} kpc and a total mass density parameter on the order of 3%. In Figure 11 we plot the expected overall filling factor (or porosity) of metal-enriched material for different scenarios, assuming a "synchronized" (over timescales shorter than the then Hubble time) population of starbursting halos. As already mentioned, with a star formation efficiency of $f_* = 10\%$, only a small fraction, about 4%, of the stars seen today would form at these early epochs. Still, the impact of such an era of pregalactic out-

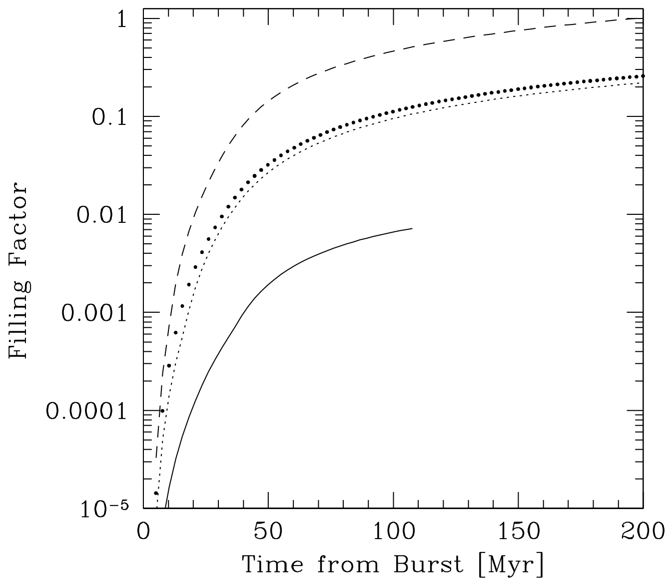

FIG. 11.—Filling factor (porosity) of the metal-enriched gas for the cases (1%, 0.1 $M_\odot$) (*solid curve*), (10%, 0.1 $M_\odot$) (*dotted curve*), (10%, 0.1 $M_\odot$), in which the halo gas mass is 50% of the standard value (*large-dotted curve*), and (50%, 0.1 $M_\odot$) (*short-dashed curve*).

flows could be quite significant since the product of stellar nucleosynthesis would be distributed over distances that are comparable to the mean proper distance between neighboring low-mass systems, i.e., filling factors $\gtrsim$20%. Larger filling factors may be obtained for larger efficiencies, moderately top-heavy IMFs, halos in which a significant fraction of the gas is in a galactic disk and does not couple to the outflow (since matter is ejected perpendicularly to the disk), or from a population of more numerous sources—which would therefore have to originate from lower amplitude peaks but which is not required by current observations. Ferrara et al. (2000) have recently considered the process of metal enrichment of the IGM, so it is useful to compare our main results with theirs. They determined the final radius of the bubbles by assuming that once blowaway has occurred, the shell enters the snowplow phase, and it is finally confined by the IGM pressure. Essentially, their stalling radius is much smaller than that derived in this work because they assumed a low cooling/star formation efficiency factor, $f_b f_* = 0.0025$ (corresponding for a halo of total mass 2×10^8 $M_\odot$ to a star formation rate of 10^{-3} $M_\odot$ yr^{-1} over 30 Myr); i.e., they studied outflows in a "quiescent" star formation mode that is perhaps more suitable to larger systems rather than to the starbursting subgalactic halos we have focused on in this work.

It is interesting to note that, following an early era of SN-driven outflows, the enriched IGM may be heated on large scales to characteristic temperatures $T_{\rm IGM} \gtrsim 10^{4.6}$ K if the star formation efficiency is $\gtrsim$10% so as to "choke off" the collapse of further $M \lesssim 3 \times 10^8$ h^{-1} $M_\odot$ systems by raising the Jeans mass. In this sense, the process may be self-regulating. While more detailed calculations—which include the contribution to the IGM metal and heat content from all levels of the mass hierarchy as a function of cosmic time—need to be done to fully assess the impact of subgalactic halos on the thermal (and ionization) state of the IGM, we argue here that it is unlikely that an early input of mechanical energy will be the dominant effect in determining the ionization state of the IGM on large scales (cf. Tegmark et al. 1993). We have shown in § 3.5 that if the fraction of ionizing photons that escapes the dense sites of star formation into the intergalactic space is greater than a few percent, pregalactic outflows will propagate into an IGM that has been prephotoionized by the same massive stars that later explode as SNe. The relative importance of photoionization versus shock ionization obviously depends on the efficiency with which radiation and mechanical energy actually escape into the intergalactic space. One can easily show, however, that, during the evolution of a "typical" stellar population, more energy is actually lost in ultraviolet radiation than in the mechanical form (see, e.g., Madau 2000). This is because in nuclear burning from zero to solar metallicity ($Z_\odot = 0.02$), the energy radiated per baryon is $0.02 \times 0.007 \times m_{\rm H} c^2$; about one-third of it goes into H-ionizing photons. While the same massive stars that dominate the UV light also explode as SNe, the mass fraction radiated in photons above 1 ryd is 4×10^{-5}, 10 times higher than the fraction released in mechanical energy. Of course, a prephotoionized universe at 10^4 K, heated up to a higher temperature by SN-driven winds, will recombine more slowly. The expected thermal history of expanding intergalactic gas at the mean density and with low metallicity is plotted in Figure 12 as a function of redshift for a number of illustrative cases. The code we use includes the relevant cooling and heating processes and follows the non-equilibrium evolution of hydrogen and helium ionic species in a cosmological context. The gas is allowed to interact with the CMB through Compton cooling and either with a time-dependent quasar-ionizing background as computed

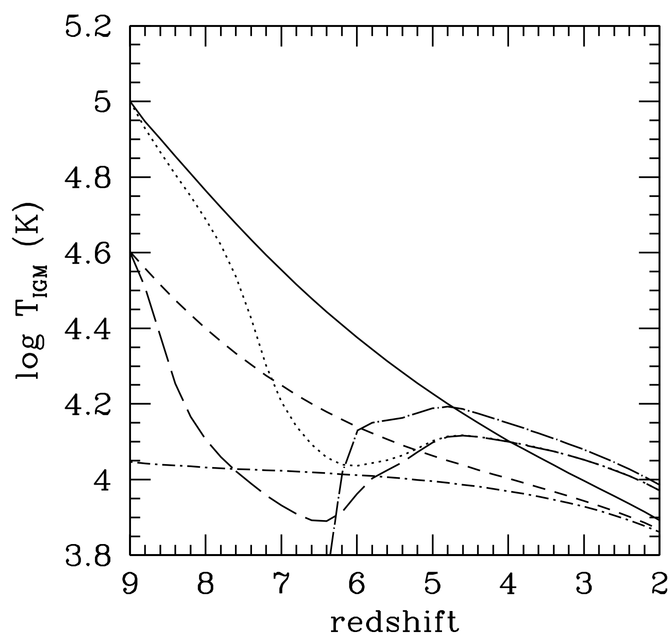

FIG. 12.—Thermal history of intergalactic gas at the mean density in an Einstein–de Sitter universe with $\Omega_b h^2 = 0.019$ and $h = 0.5$. *Short–dash-dotted line:* Temperature evolution when the only heating source is a constant ultraviolet (CUV) background of intensity 10^{-22} ergs cm^{-2} s^{-1} Hz^{-1} sr^{-1} at 1 ryd and a power-law spectrum with energy slope $\alpha = 1$. *Long–dash-dotted line:* Same as the time-dependent quasar-ionizing background as computed by Haardt & Madau (1996, hereafter HM). *Short-dashed line:* Heating due to a CUV background, but with an initial temperature of 4×10^4 K at $z = 9$ as expected from an early era of pregalactic outflows. *Long dashed line:* Same as the short-dashed curve but for a HM background. *Solid line:* Heating due to a CUV background, but with an initial temperature of 10^5 K at $z = 9$. *Dotted line:* Same as the solid line, but for a HM background.

by Haardt & Madau (1996) or with a time-independent metagalactic flux of intensity 10^{-22} ergs cm^{-2} s^{-1} Hz^{-1} sr^{-1} at 1 ryd (and a power-law spectrum with energy slope $\alpha = 1$). The temperature of the medium at $z = 9$—where we start our integration—has been either computed self-consistently from photoheating or fixed to be in the range $10^{4.6}$–10^5 K expected from SN-driven bubbles with significant filling factors. The various curves show that the temperature of the IGM at $z = 3$–4 will retain little memory of an early era of pregalactic outflows.

Support for this work was provided by NASA through ATP grant NAG 5-4236 and grant AR-06337.10-94A from the Space Telescope Science Institute (P. M.), by a B. Rossi Visiting Fellowship at the Observatory of Arcetri (P. M.), by the Center for Computational Physics at Tsukuba University (A. F.), and by the Royal Society (M. J. R.). A. F., P. M., and M. J. R. also acknowledge the support of the EC RTN network "The Physics of the Intergalactic Medium."

REFERENCES

Abel, T., Anninos, P., Zhang, Y., & Norman, M. L. 1997, NewA, 2, 181
Abel, T., Bryan, G. L., & Norman, M. L. 2000, ApJ, 540, 39
Aguirre, A., Schaye, J. Hernquist, L., Weinberg, D., Katz, N., & Gardner, J. 2000, ApJ, submitted (astro-ph/0006345)
Barkana, R., & Loeb, A. 1999, ApJ, 523, 54
———. 2001, Phys. Rep., in press
Barnes, J., & Efstathiou, G. 1987, ApJ, 319, 575
Bullock, J. S., Kolatt, T. S., Sigad, Y., Somerville, R. S., Kravtsov, A. V., Klypin, A. A., Primack, J. R., & Dekel, A. 2001, MNRAS, 321, 559
Burles, S., & Tytler, D. 1998, ApJ, 499, 699
Cen, R., Miralda-Escudé, J., Ostriker, J. P., & Rauch, M. 1994, ApJ, 437, L9
Ciardi, B., Ferrara, A., & Abel, T. 2000, ApJ, 533, 594
Couchman, H. M. P., & Rees, M. J. 1986, MNRAS, 221, 53
Cowie L. L., & McKee, C. F. 1977, ApJ, 211, 135
Cowie, L. L., & Songaila, A. 1998, Nature, 394, 44
Dekel, A., & Silk, J. 1986, ApJ, 303, 39
Efstathiou, G. 1992, MNRAS, 256, 43P
———. 2000, MNRAS, 317, 697
Ellison, S. L., Songaila, A., Schaye, J., & Pettini, M. 2000, AJ, 120, 1175
Ferrara, A., Pettini, M., & Shchekinov, Y. 2000, MNRAS, 319, 539
Ferrara, A., & Shchekinov, Yu. 1993, ApJ, 417, 595
Fukugita, M., Hogan, C. J., & Peebles, P. J. E. 1998, ApJ, 503, 518
Gnedin, N. Y. 1998, MNRAS, 294, 407
———. 2000, ApJ, 542, 535
Gnedin, N. Y., & Ostriker, J. P. 1997, ApJ, 486, 581
Gull, S. F. 1973, MNRAS, 161, 47
Haardt, F., & Madau, P. 1996, ApJ, 461, 20 (HM)
Haiman, Z., Abel, T., & Madau, P. 2001, ApJ, 551, 599
Haiman, Z., Abel, T., & Rees, M. J. 2000, ApJ, 534, 11
Haiman, Z., Rees, M. J., & Loeb, A. 1996, ApJ, 467, 522
Heckman, T. M. 1999, in AIP Conf. Proc. 470, After the Dark Ages: When Galaxies Were Young, ed. S. S. Holt & E. P. Smith (Woodbury: AIP), 322
Heiles, C. 1990, ApJ, 354, 483
Hernquist, L., Katz, N., Weinberg, D., & Miralda-Escudé, J. 1996, ApJ, 457, L51
Hui, L., & Gnedin, N. Y. 1997, MNRAS, 292, 27
Kim, T.-S., Hu, E. M., Cowie, L. L., & Songaila, A. 1997, AJ, 114, 1
Kompaneets, A. S. 1960, Soviet Phys. Dokl., 5, 46
Larson, R. B. 1974, MNRAS, 169, 229
Machacek, M. E., Bryan, G. L., & Abel, T. 2001, ApJ, 548, 509
Mac Low, M.-M., & Ferrara, A. 1999, ApJ, 513, 142
Mac Low, M.-M., & McCray, R. 1988, ApJ, 324, 776
Madau, P. 2000, Philos. Trans. R. Soc. London A, 358, 2021
Madau, P., & Efsthathiou, G. 1999, ApJ, 517, L9
Madau, P., & Rees, M. J. 2000, ApJ, 542, L69
Makino, N., Sasaki, S., & Suto, Y. 1998, ApJ, 497, 555
Martin, P. G., Schwarz, D. H., & Mandy, M. E. 1996, ApJ, 461, 265
Mather, J. C., Fixsen, D. J., Shafer, R. A., Mosier, C., & Wilkinson, D. T. 1999, ApJ, 512, 511
McKee, C. F., & Begelman, M. C. 1990, ApJ, 358, 392
McKee, C. F., & Ostriker, J. P. 1977, ApJ, 218, 148
Murakami, I., & Babul, A. 1999, MNRAS, 309, 161
Nath, B., & Trentham, N. 1997, MNRAS, 291, 505
Navarro, J. F., Frenk, C. S., & White, S. D. M. 1997, ApJ, 490, 493 (NFW)
Omukai, K., & Nishi, R. 1999, ApJ, 518, 64
Ostriker, J. P., & McKee, C. F. 1988, Rev. Mod. Phys., 60, 1
Pettini, M., Steidel, C. C., Adelberger, K. L., Dickinson, M., & Giavalisco, M. 2000, ApJ, 528, 96
Press, W. H., & Schechter, P. 1974, ApJ, 187, 425 (PS)
Ricotti, M., Gnedin, N. Y., & Shull, J. M. 2000, ApJ, 534, 41
Ryan, S. G., Norris, J. E., & Beers, T. C. 1996, ApJ, 471, 254
Scannapieco, E., & Broadhurst, T. 2001, ApJ, 549, 28
Schaerer, D., & de Koter, A. 1997, A&A, 322, 598
Schaller, G., Schaerer, D., Meynet, G., & Maeder, A. 1992, A&AS, 96, 269
Schaye, J., Rauch, M., Sargent, W. L. W., & Kim, T.-S. 2000, ApJ, 541, L1
Songaila, A. 1997, ApJ, 490, L1
Songaila, A., & Cowie, L. L. 1996, AJ, 112, 335
Steidel, C. C., Adelberger, K. L., Giavalisco, M., Dickinson, M., & Pettini, M. 1999, ApJ, 519, 1
Sutherland, R. S., & Dopita, M. A. 1993, ApJS, 88, 253
Tegmark, M., Silk, J., & Evrard, A. 1993, ApJ, 417, 54
Tegmark, M., Silk, J., Rees, M. J., Blanchard, A., Abel, T., & Palla, F. 1997, ApJ, 474, 1
Theuns, T., Leonard, A., Efstathiou, G., Pearce, F. R., & Thomas, P. A. 1998, MNRAS, 301, 478
Theuns, T., Mo, H. J., & Schaye, J. 2001, MNRAS, 321, 450
Thoul, A. A., & Weinberg, D. H. 1996, ApJ, 465, 608
Todini, P., & Ferrara, A. 2000, MNRAS, submitted (astro-ph/0009176)
Vacca, W. D., Garmany, C. D., & Shull, J. M. 1996, ApJ, 460, 914
Voit, G. M. 1996, ApJ, 465, 548
Weaver, R., McCray, R., Castor, J., Shapiro, P., & Moore, R. 1977, ApJ, 218, 377
White, S. D. M., & Frenk, C. S. 1991, ApJ, 379, 52
White, S. D. M., & Rees, M. J. 1978, MNRAS, 183, 341
Wood, K., & Loeb, A. 2000, ApJ, 545, 86
Woosley, S. E., & Weaver, T. A. 1995, ApJS, 101, 181
Zhang, Y., Anninos, P., & Norman, M. L. 1995, ApJ, 453, L57
Zhang, Y., Meiksin, A., Anninos, P., & Norman, M. L. 1998, ApJ, 495, 63